Demonstration of continuous multiple access with homodyne and image-rejection heterodyne coherent receivers using DML transmitters

MIQUEL MASANAS[1*], JEISON TABARES[1,2], IVAN CANO[3], JOSEP PRAT[1]

[1]*Department of Signal Theory and Communications, Universitat Politècnica de Catalunya, 08034, Barcelona, Spain*
[2]*Luxquanta Technologies, Carl Friedrich Gauss 3, 08860, Castelldefels, Spain*
[3]*Munich Research Centre, Huawei Technologies*
**Corresponding author: miquel.masanas@upc.edu*

Received XX Month XXXX; revised XX Month, XXXX; accepted XX Month XXXX; posted XX Month XXXX (Doc. ID XXXXX); published XX Month XXXX

This work presents a comprehensive set of experiments for multipoint to point coherent PON, where the wavelength locking between ONU and OLT lasers is critical, especially if operating in burst mode. Here, we test the performance of continuous multiple access in a splitter-based PON with both a UD-WDM and RF-subcarrier multiplexing (SCM) configuration, with simple distributed feedback lasers along NRZ and PAM-4 modulation. Most interestingly, we test a spectrally-efficient heterodyne receiver with image-frequency rejection and polarization independence based on the 3x3 optical front-end. Two users at the same IF are detected simultaneously avoiding image frequency interference while minimizing complexity, with transmissions of 2.5 Gb/s. We provide comparison with a homodyne receiver. The achieved results demonstrate the feasibility of continuous multiple access using thermally controlled ONUs with conventional DFBs, as enhanced alternative to commercial TDM access.

http://dx.doi.org/10.1364/JOCN.99.099999

1. Introduction

Optical local area networks can find applications for industrial and critical machine communications, as they offer high reliability and robustness against electromagnetic interference. Also, industrial and RF networks can have a high number of terminals like sensors and actuators which might not transmit a high speed but need low and deterministic latency [1-3]. To reduce the cost of the network, a point-to-multipoint architecture can be used [4]. In addition, the transceivers should be simple to keep the footprint and complexity as low as possible. To address these requirements, coherent-lite schemes might be a key-enabling technology as they enhance the optical power budget and allow for filter-less ultra-dense wavelength division multiplexing (UD-WDM) which can bring significant latency reduction and reliability. The general objective of this work is to build a multi-user access, splitter-based passive optical network (PON) with many coexisting distributed low-cost light sources emitting at extremely-close optical frequencies.

In this work we propose continuous multiple access (CMA), avoiding TDM/TDMA schemes, to deliver latency and reliability requirements to as many optical network units (ONUs) as possible. For this, IM/DD schemes are not suitable in absence of optical filtering. Coherent detection enables to avoid time multiplexing over splitter-based PON and transceivers through UD-WDM schemes, while also being the solution with highest sensitivity. However, the usual cost and complexity off conventional coherent schemes is not suitable for edge networks, with high ubiquity of terminations and hardware. To reduce the complexity of a conventional coherent network, at the OLT we target a single local oscillator for as many ONUs as possible. To achieve this, at the OLT receiver (RX), placed at the central aggregation point of the network, we compare the performance of two RX. On the one hand, a polarization-independent heterodyne detection with image-frequency cancellation, to simultaneously detect two users at both sides of the local oscillator (LO), thus doubling the spectral efficiency and lowering the needed electrical bandwidth (BW) of the RX. On the other hand, we compare it with a conventional homodyne 3x3 front-end with the users multiplexed in electrical frequency. At the TX we investigate the performance of DML-IM, which uses the simplest electro-optical infrastructure possible.

For the tests, we directly modulated NRZ and PAM-4 both in base-band (BB) and over RF in a sub-carrier multiplexing (SCM) configuration.

The document is organized as follows: Section 2 summarizes the targeted network characteristics and the different options to achieve it. Section 3 provides detail on the polarization-independent heterodyne detection with image-frequency cancellation, proposed as the an interesting tool to achieve the target. Section 4 presents comprehensive experiments of the DML TX in baseband and RF configurations, both in NRZ and PAM-4 modulations, and both with square pulse-shaping and Nyquist pulse shaping. Section 5 presents comprehensive experiments on CMA for 2 simultaneous users, using the conventional coherent homodyne RX used in Section 4, as well as the novel RX presented in Section 3. Finally, Section 6 provides the conclusions of the work.

2. Network architecture

A. Modulations case studies

In order to achieve CMA in coherent PON, there are two main conventional approaches at the TXs: either they use different wavelengths and baseband (BB) modulation in a UD-WDM scheme, corresponding to Figure 1 (a), or they use the same central wavelength and use RF modulation over different frequencies, thus resulting in a

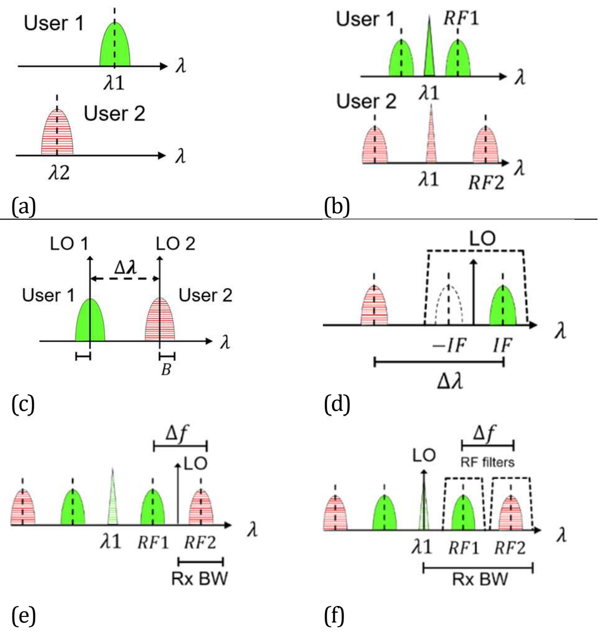

Fig. 1: (a) Baseband modulation of two users in different wavelengths (b) RF modulation of two users in two lasers over the same wavelength (c) Homodyne detection of the scenario in (a). (d) Heterodyne detection of the scenario in (a). (e) Heterodyne detection of the scenario in (b). (f) Homodyne detection of the scenario in (b).

SCM configuration, depicted in Figure 1 (b). For each approach to the TX, the RX can be either homodyne or heterodyne. The BB TX – homodyne RX (BB-homodyne, Figure 1 (c)) approach has a 1:1 LO-TX relationship, which is not scalable for termination-dense networks. BB-conventional heterodyne (Figure 1 (d)) has its spectral and electrical bandwidth efficiencies limited by the image frequency interference. SCM along with conventional heterodyne (Figure 1(e)) would need increased modulation RF frequencies to avoid image interference. Finally, SCM-homodyne (Figure 1(f)) is able to achieve the CMA target, although with a very high RX bandwidth when increasing the termination count.

However, if we consider image rejection (IR) at the heterodyne RX, there are notable improvements for both TXs scenarios. Such a RXs avoids image frequency interference between channels located opposite sides of the LO, thus being able to share IF frequency. Also, by separately recovering both sides of the LO, we can detect two channels using the same LO and electrical RX bandwidth. On the one hand, this means that using BB TXs and the IR-heterodyne RX leads to the same spectral efficiency as conventional BB-homodyne, but potentially using half of the LOs. On the other hand, when using SCM TXs, the LO can be placed between user bands (Figure 2 (a)), detecting both at the same time and reducing electrical requirements, as the image frequency is not interfering and RF frequencies can be lower. This makes practical a SCM transmitter with a heterodyne RX.

Section 3 provides further detail on the IR-heterodyne architecture studied, first proposed in [5], to achieve the SCM-heterodyne scenario.

3. Image rejection heterodyne 3x3 RX

The key idea is to use an optical heterodyne coherent RX based on a 3x3 optical coupler, shown in Figure 2 (b), which aided by electrical signal processing realized either by DSP or analog hardware, rejects the image-frequency band of the heterodyne detection. In this way, two different signals separated in wavelength –or equivalently in RF frequency– can be simultaneously detected by the same coherent RX within the same electrical BW.

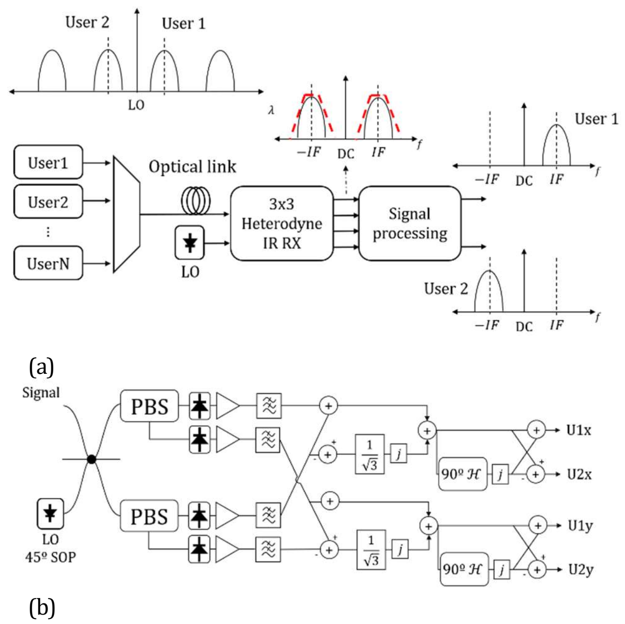

Fig. 2: (a) Simultaneous detection of two different users using an optical heterodyne image-rejection RX (b) 3x3 heterodyne image-rejection RX: optical front-end and electrical signal processing.

Additionally, the incoming optical signals can have random polarization states and still be detected by the novel heterodyne RX front-end, composed by the 3x3 optical coupler, polarization beam splitters (PBSs), and the LO with a specific polarization. Hence, two users can be detected simultaneously with a single RX with total independence from the received polarizations. At the optical front-end, the 3x3 coupler mixes the received signal with the LO, which is optimally polarized at 45º for symmetric polarization-diversity. The resulting optical beatings from two of the three branches are split into two orthogonal polarization components $\mathbb{X}$, $\mathbb{Y}$ by a pair of PBSs, then photodetected by four single-ended PDs. The third branch of the 3x3 coupler is unused. After photodetection, the four signals are band-pass filtered and delivered to the electrical signal processing part of the RX.

First, both I and Q components for each polarization are recovered by a simple linear combination of the four photocurrents. Next, the image-rejection part of the RX exploits the fact that the Q signal is sensitive to the sign of the frequency difference between the two different users and the LO, as both are symmetrically placed at opposite sides from the LO. The result is that the frequency spectrum of the complex signal I+jQ for each polarization contains the detected User1 and User2 at positive and negative frequencies, respectively, without spectral overlap (see Figure 23 insets). Therefore, to reject interference from one user to the other –namely the image frequency band–, we need to isolate the positive and the negative single-sidebands (SSB) of the signals $X(t) = I(t) + jQ(t)$ for each polarization. This can be realized using a pair of Hilbert transforms $\mathcal{H}\{\cdot\}$, as illustrated in Figure 23, by implementing the expression:

$$X_{SSB}(t) = X(t) \pm j\mathcal{H}\{X(t)\} \tag{1}$$

This can be done either digitally or analogically. This RX achieves phase and polarization diversity in a reduced-cost and complexity structure. Moreover, it has a theoretical 3 dB sensitivity improvement with respect the conventional heterodyne, by cancelling half of the noise band. Finally, the individual detected signals for each user with polarization diversity are demodulated by e.g., envelope detection for intensity modulation formats, and later combined to counteract changes in the received polarizations after propagation through the optical fiber link.

4. Direct laser modulation tests

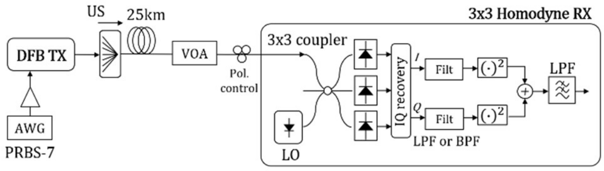

Fig. 3: Experimental setup for direct laser modulation with coherent homodyne detection

This section now focuses on the direct modulation tests using off the shelf DFB lasers. The modulation formats are NRZ and 4-level PAM, both evaluated in baseband and RF modulation, and the RX is the standard single-polarization homodyne front-end based on the 3x3 optical coupler. For the modulation quality analysis, the test are done for a single user scenario.

A. Experimental set up

As previously said, the RX type is coherent with 3x3 homodyne front-end, single-polarization, as depicted in Figure 3. The lasers temperatures were set to 35ºC while the room temperature was 25ºC. At the TX, the data were generated by an AWG that performed bit-to-symbol mapping for the case of PAM-4, and spectral shaping with both square pulses and raised-cosine filter. The lasers were biased at 40 mA, and the modulated optical signal –representing the US transmission– was transmitted through 25 km of SSMF towards the coherent RX.

At the RX input, a variable optical attenuator (VOA) adjusted the received signal power, and the state-of-polarization (SOP) was manually adjusted. The LO was an ECL emitting at 3 dBm. The received signal was detected by the 3x3 homodyne RX, and the electrical in-phase (*I*) and quadrature (*Q*) signals were recovered and filtered by LPF for the case of baseband modulation, or by BPF for RF modulation. The *IQ* recovery block also cancels the DD terms and the common-mode noise. Last, the signals were squared for envelope detection and low-pass filtered before data decision.

The modulation BWs and the RF frequencies were mainly limited by the frequency response of the DML. For the case of the lasers used, referred as Laser 1 and Laser 2, and biased at 40 mA in our tests, the modulation BWs at -3 dB are about 4.5 and 6 GHz respectively. In what follows, the DML performances with coherent detection are presented, and the main outcomes and key parameters for their application in an optical access scenario are summarized and discussed.

B. Baseband modulation

In this scenario, the tested modulation BW is 1.25 GBd that translates into 1.25 and 2.5 Gb/s per wavelength, for NRZ and PAM-4 respectively. The Nyquist spectral shaping was done electrically at the TX and before the optical modulation, with a raised-cosine FIR filter with roll-off 0.5 and 1. The RX filter was low-pass 4^{th}-order Bessel with variable cut-off frequency because of the extra required BW in homodyne detection using DMLs due to the laser chirp spectrum spreading, as it will be discussed later. Many optical transmission systems use matched filtering at the TX/RX by square-root-raised-cosine filters; here, though, the RX implements standard LPF to lower the RX complexity.

1. 1.25 Gb/s NRZ

The BER as a function of the received optical power was computed for different modulation indexes *m*, and three different pulse-shapes of the modulating current: square and Nyquist with roll-off 0.5 and 1. The results are plotted in Figure 4. In all cases, the larger is the modulation index the higher is the RX sensitivity. Concretely, for BER = 10^{-3} the

Table 1

		BER = 10-3	Error-free
Pulse shape	Square	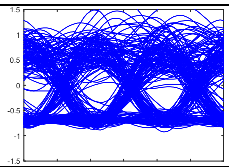	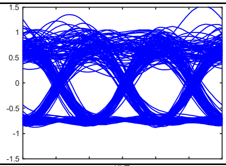
	Raised cosine roll-off = 1	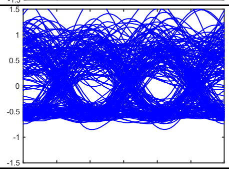	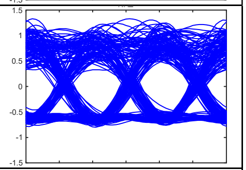
	Raised cosine roll-off = 0.5	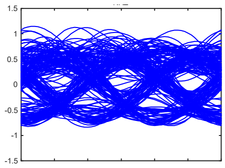	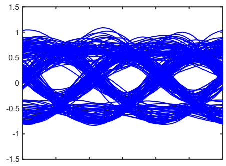

highest sensitivity (with *m* = 0.8) was -49 dBm for square pulse-shape, -48.5 dBm and -47 dBm for raised-cosine pulse-shape with roll-off 1 and 0.5 respectively. The power penalty that arises after Nyquist shaping originates in part by the unmatched TX-RX filtering, and in part by the slight eye closure caused by the raised-cosine filtering, as appreciated in the eye diagrams in Table 1 for error-free detection and BER = 10^{-3}.

Another important behavior in each plot of Figure 4, worth to be mentioned, is that the sensitivity penalty among the curves with different m reduces for Nyquist shaping compared with square pulse-shape. This can be ascribed to the different requirements in RX BW due to the laser chirp spectrum spreading, as summarized in Table 2. For square pulse-shape, sweeping m from 0.8 to 0.2 reduces the required RX BW from 4RB to 1.4RB, where RB is the baud rate. In contrast, for raised-cosine with roll-off = 0.5 –the narrowest modulated spectrum– the required RX BW ranges from 2.8RB to 0.8RB for m = 0.8 and 0.2 respectively. This represents in between 30% and 40% RX BW reduction when using Nyquist shaping, and therefore, the in-band noise of the detected signal is lower.

Table 2

	Required RX BW (GHz)		
m	Square	Raised cosine roll-off = 1	Raised cosine roll-off = 0.5
0.2	1.8	1.5	1
0.4	2.5	2	1.5
0.6	3.5	2.5	2
0.8	5	4	3.5

From the tests, it can be derived that the election of the modulation index *m* presents a trade-off between RX sensitivity and modulated spectrum width. Lower *m* shows spectrum compactness but raises a penalty in RX sensitivity, whereas higher *m* reaches high sensitivity but requires significantly larger RX BW and optical channel spacing.

The highest RX sensitivity achieved here using coherent homodyne detection, of -49 dBm for *m* = 0.8 with NRZ at 1.25 Gb/s, outperforms by 13 dB the sensitivity of actual standards for PON using conventional DD RXs, reported to be -36 dBm at 1.25 Gb/s, the lowest for E2 class ODN [6]. Furthermore, it is only 6 dB lower than the high sensitivity reported in [7] for direct DPSK modulation at 1.25 Gb/s (of -55 dBm), the benchmark for coherent homodyne detection.

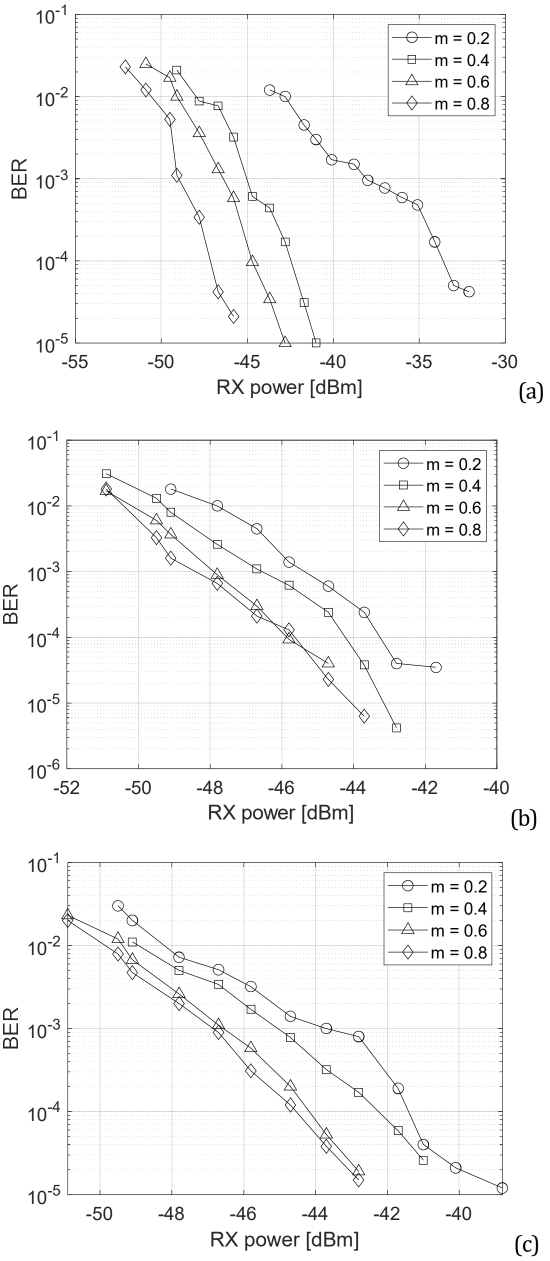

Fig. 4: BER vs. RX power for 1.25 Gb/s NRZ with several modulation indexes, and with three different pulse-shapes: (a) square, and raised-cosine with (b) roll-off =1, and (c) roll-off = 0.5.

2. 2.5 Gb/s PAM-4

The second baseband modulation test is PAM-4 at R_B = 1.25 GBd, i.e., 2.5 Gb/s. The data were demodulated at the RX by envelope detection, as shown in Figure 3 and similarly to the previous NRZ experiment. Here, though, a real-valued 4-tap FIR equalizer was placed at the RX after photodetection and before envelope detection for mitigation of the ISI and enhancement of the eye diagram opening. The filter taps were experimentally adjusted to emphasize the proper frequencies after comparing the ideal transmitted and the received PAM-4 symbols. The BER performances are plotted in Figure 5 with square and raised-cosine pulse shape.

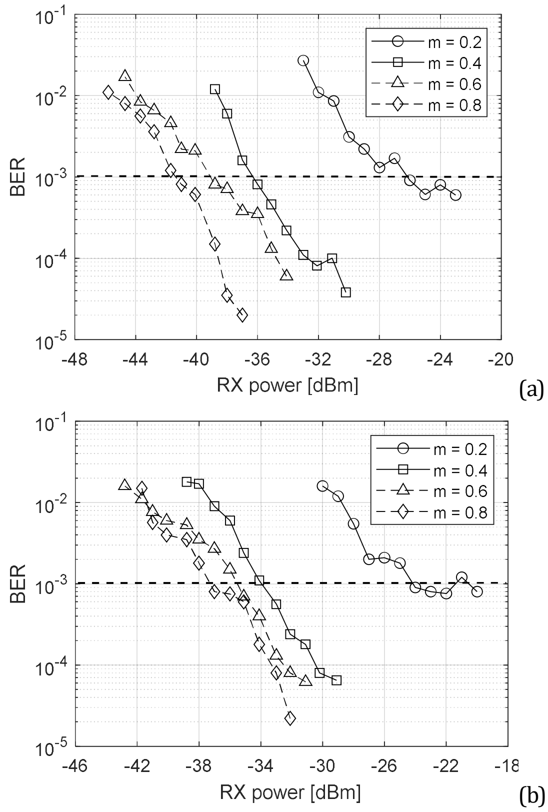

Fig. 5: BER vs. RX power for 2.5 Gb/s PAM-4 with several modulation indexes, and with (a) square pulse-shape and (b) raised-cosine with roll-off = 1.

The highest PAM-4 sensitivity at BER = 10^{-3}, achieved for m = 0.8, is -42 dBm and -37.5 dBm for square pulse-shape and raised-cosine with roll-off = 1 respectively. The higher the m, the better is the RX sensitivity. Compared with the NRZ at the same R_B, and considering square pulse-shape, the sensitivity penalty is about 8 dB for all the tested m, except for m = 0.2 that shows >10 dB penalty and apparent error-floor around 10^{-3} BER. For the case of raised-cosine with roll-off = 1, the mean penalty against NRZ raises to 12 dB, due to the eye closure caused by the Nyquist filtering. This can be appreciated in the eye diagrams in Table 3.

Table 3

		BER = 10^{-3}	Error-free
Pulse shape	Square	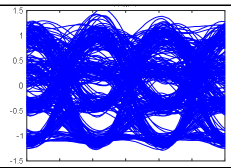	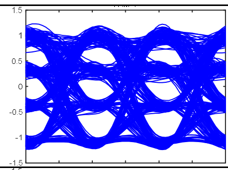
Pulse shape	Raised cosine roll-off = 1	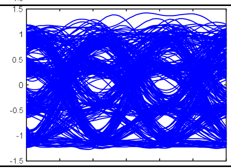	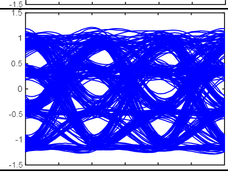

It should be mentioned that the BER results for raised-cosine pulse-shape with roll-off = 0.5 were not computed because significant eye closure was observed, also with error-floor near to BER = 10^{-2}, even for large modulation index. Furthermore, the complete eye opening and the error-free detection of the PAM-4 signals were only achieved after the 4-tap FIR equalization; otherwise, without the FIR the eye diagram was partially closed because the multilevel PAM modulation is more

	Table 4	
	Required RX BW (GHz)	
m	Square	Raised cosine roll-off = 1
0.2	2	2
0.4	2.5	2
0.6	3.5	2.5
0.8	5	4.5

sensitive to non-ideal frequency response of the transmission path including laser, amplifiers and photodiodes.

The required RX BWs for homodyne detection of PAM-4 are summarized in Table 4. Note that the results in the table are only slightly larger than the NRZ modulation, and therefore, the sensitivity penalty when varying *m* in Figure 5 is larger for square pulse-shape than raised-cosine because of the larger RX BW, similar to the NRZ tests.

Finally, the performance of PAM-4 with coherent detection can be compared with the results reported in [8] for 2.5 Gb/s QPSK using direct laser chirp modulation. For BER = 10^{-3} the QPSK achieved -47 dBm sensitivity, 5 dB better than the PAM-4 in our tests. However, larger optical channel spacing is expected for PAM-4 compared with QPSK because of the laser chirp spectrum spreading (see section 5).

C. RF modulation

The second scenario focuses on SCM through optical modulation with RF carriers. In this case, the BW of the lasers previously reported dictates the maximum RF frequency and the symbol rate R_B. Since lasers 1 and 2 are limited in BW to 4.5 and 6 GHz respectively, the tested RF frequencies ranged from 1.25 to 3.75 GHz, and R_B was set to 625 MBd.

At the homodyne RX after photodetection, the filtering was band-pass implemented as 3rd-order Bessel high-pass + 4th-order Bessel low-pass, both with cut-off frequency at $0.9R_B$, as in Figure 6(a) Interestingly, this band-pass filter BW was optimal for the two tested modulation indexes (*m* = 0.4 and 0.6) and for all the RF frequencies. This contrasts with the baseband modulation tests in previous sections where the RX BW increased for larger *m* due to the chirp spreading. The reason is that in the FM modulation produced by the laser chirp, the FM modulation index $\beta = \Delta f / f_m$ lowers when the modulation frequency f_m increases, and therefore the modulated spectrum is narrower. Here Δf is the optical frequency variation due to the chirp parameter of the laser, and relates to the amplitude of the modulation current swing.

1. 1.25 Gb/s NRZ

Here the DML was modulated with NRZ data at 625 MBd on electrical RF carriers at {1.25, 2.5, 3.75} GHz. The BER performances for optical homodyne detection are plotted in Figure 18 for two pulse-shapes: square and raised-cosine with roll-off = 1.

The best RX sensitivity at BER = 10^{-3} was -45.5 and -44.5 dBm for square pulse-shape and raised-cosine with roll-off = 1 respectively, with *m* = 0.6. The power penalty between the curves in Figure 7 (a) for square pulse-shape and Figure 7 (b) for raised-cosine, for the same *m* and RF frequency, is about 1dB, which is in good agreement with the previous baseband modulation tests. On the other hand, in all cases the power penalty for varying *m* from 0.6 to 0.4 is <1 dB. Regarding the RF frequency, the best RX sensitivity was achieved for the lowest f_{RF} = 1.25 GHz, with about 3 dB better sensitivity than f_{RF} = 3.75 GHz in both figures, mostly caused by the non-ideal frequency response of the DFB and RF components at higher frequencies that leads to signal distortion.

The obtained electrical spectrum at the RX for *m* = 0.6 is depicted in Figure 7 for the two different pulse shapes and f_{RF} = 2.5 GHz. As

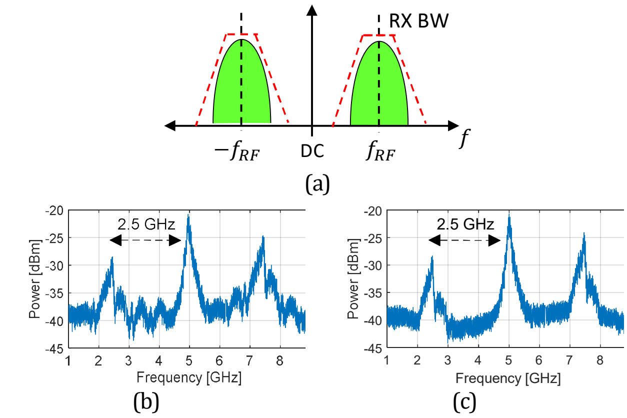

Fig. 6: (a) Scheme of the electrical spectrum at the RX after homodyne detection. Experimental spectrum at the RX centred at 5 GHz, for m = 0.6, f_RF = 2.5 GHz, R_B = 625 MBd, with (b) square pulse-shape and (b) raised-cosine pulse-shape with roll-off = 1.

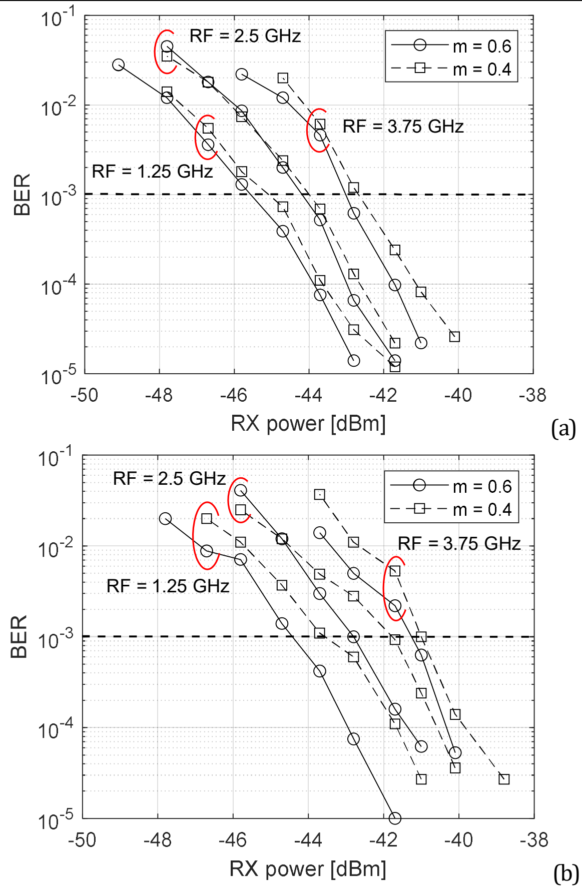

Fig. 7: BER vs. RX power for 625 Mb/s RF-NRZ with different RF frequencies, and with (a) square pulse-shape and (b) raised-cosine with roll-off = 1.

expected, the use of Nyquist pulse-shaping in Figure 6(c) completely eliminates the modulation secondary lobes when comparing with square pulse-shape in Figure 6(b). This is advantageous to reduce the interference to adjacent RF users multiplexed in SCM. It is also worth to note that each of the modulated side-bands in Figure 6 (b) and (c) exhibit partial cancellation of one side of the main modulation lobe. This originates from the simultaneous amplitude and frequency modulation of the DML under injection current modulation, due to the laser chirp;

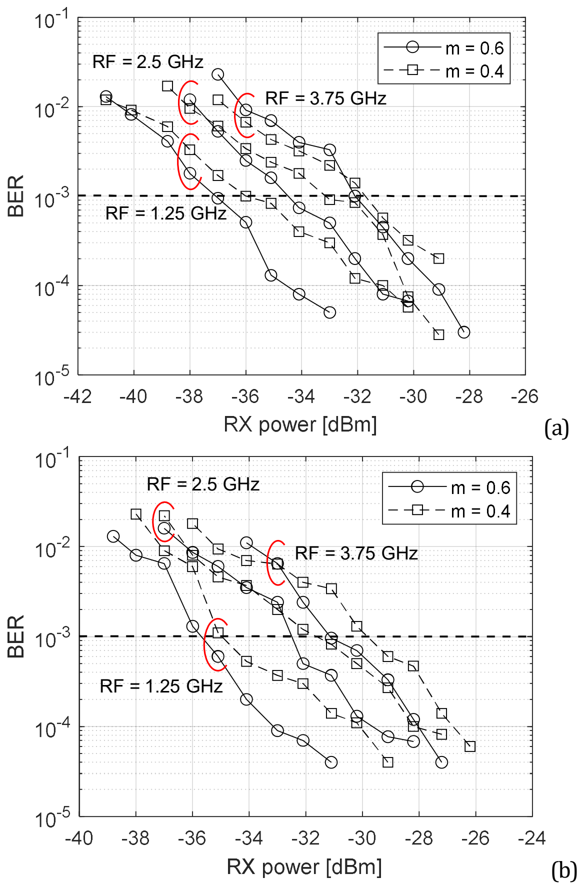

Fig. 8: BER vs. RX power for 1.25 Gb/s RF-PAM-4 with different RF frequencies, and with (a) square pulse-shape and (b) raised-cosine with roll-off = 1.

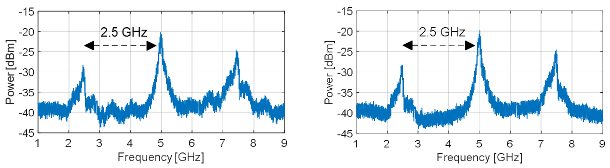

Fig. 9: Experimental spectrum at the RX centered at 5 GHz, for m = 0.6, f_RF = 2.5 GHz, R_B = 625 MBd, with (a) square pulse-shape and (b) raised-cosine pulse-shape with roll-off = 1.

thus, some harmonics of the AM and FM modulation compete in counterphase producing spectrum cancellation. This phenomenon is driven by the modulation index *m*, and can be potentially exploited to generate single side-bands (SSB) signals for RF TXs.

2. 2.5 Gb/s PAM-4

The last single-user test consisted of PAM-4 at 625 MBd, i.e. 1.25 Gb/s, on electrical RF carriers at {1.25, 2.5, 3.75} GHz, similar to the NRZ in previous section. The detection scheme is also homodyne with band-pass RF filtering for channel selection. Figure 8 presents the computed

BER as a function of the received optical power for RF-PAM-4 with square pulse-shape and raised-cosine with roll-off = 1.

The RF-PAM-4 also achieved high performance, with RX sensitivity of -37 and -35.5 dBm at BER = 10^{-3}, for square pulse-shape and raised-cosine with roll-off =1 respectively, with m = 0.6 and f_{RF} = 1.25 GHz. These sensitivities are correspondingly 8 and 9 dB worse than the RF-NRZ in previous section 4.C.1, in good agreement with the 8 dB power penalty found between NRZ and PAM-4 baseband tests. The power penalty for reducing m from 0.6 to 0.4 is <1 dB in all cases, similar to RF-NRZ, but the penalty when varying f_{RF} from 1.25 to 3.75 GHz is now 5 dB, because the impact of the non-ideal response of the lasers, amplifiers, and RF components causing ISI and signal distortion is more severe in PAM-4 than in NRZ, as stated before.

The photodetected spectrum at the RX for PAM-4 is quite similar to that the NRZ modulation, for equivalent m, R_B and f_{RF}, as observed in Figure 9. The partial modulated side-band cancellation is also evident in the PAM-4 spectrum.

5. Continuous multiple access in coherent PON

The final part of the project targets the demonstration of continuous multiple access, using coherent detection and the complexity reduced IR-heterodyne front end from section 3. The objective is to evaluate an improved alternative to conventional access by TDM with DD, in terms of spectral efficiency, RX sensitivity, net bit rate, and energy consumption. As a further benefit, the continuous operation of the lasers without data burst relaxes the requirements of the wavelength and temperature stabilization system of the lasers.

Based on the modulation tests reported in section 4 with NRZ and PAM-4, along with the novel coherent heterodyne image-rejection RX introduced in section 3, two different scenarios for the demonstration of continuous multiple access were considered and experimentally assessed:

- Ultra-dense wavelength division multiplexing, with dedicated wavelength per user and baseband modulation.
- Subcarrier multiplexing through RF subcarriers modulation. The users emit at the same wavelength.

The two scenarios were evaluated using lasers 1 and 2 as User 1 and User 2, respectively, both emitting at -1 dBm. For direct laser modulation, the modulation index m was set to 0.6 in all cases, and the pulse-shaping filter of the modulating data was raised-cosine with roll-off = 1. At the RX side, the two users were detected *simultaneously* by the coherent RX based on 3x3 optical coupler, either with homodyne or IR-heterodyne detection, depending on the tested scenario. The following sections explain in detail the experimental setup and the key results.

A. Baseband modulation

The first scenario is UD-WDM access, depicted in Figure 10. Each user modulated baseband data at R_B = 1.25 GBd, with two modulation formats: NRZ and PAM-4. The coherent RX type was the 3x3 heterodyne image-rejection shown in Figure 2 (b), polarization-independent, which is able to detect the two users simultaneously by locating them symmetrically at both sides of the LO. Therefore, the wavelength separation between users is $\Delta\lambda = 2IF$, where IF is the intermediate frequency of the heterodyne detection. In our specific test, the IF was initially set to $2R_B$ = 2.5 GHz, then $\Delta\lambda$ = 5 GHz. The experimental electrical spectra at the RX after simultaneous detection of User 1 and User 2 are plotted in Figure 11 for NRZ data at 1.25 Gb/s. The plotted spectra correspond to the recovered complex *I+jQ* signal for each polarization. In Figure 11.a User 1 and User 2 are emitting unmodulated light, and the coherent RX correctly detects each user at negative and positive electrical frequencies respectively. Next, User 2 was modulated with NRZ at 1.25 Gb/s in Figure 11.b. Note that the modulated spectral width is significantly larger than R_B because of the laser chirp spreading (in our tests, m = 0.6). In Figure 11.c both users are modulated with similar NRZ data at 1.25 Gb/s, uncorrelated in time. Finally, Figure 11.d shows the spectrum after image-rejection to cancel the interference from User 1, with more than 40 dB rejection of User 1 by DSP.

The BER performance of the two users detected simultaneously by the same 3x3 heterodyne image-rejection RX is reported in

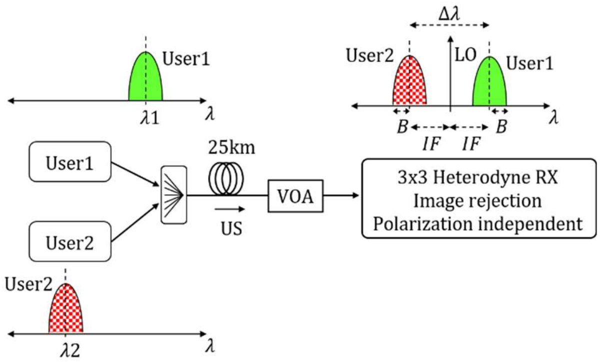

Fig. 10: Continuous multiple access with two UD-WDM users modulated in baseband and detected simultaneously by the 3x3 heterodyne image-rejection RX.

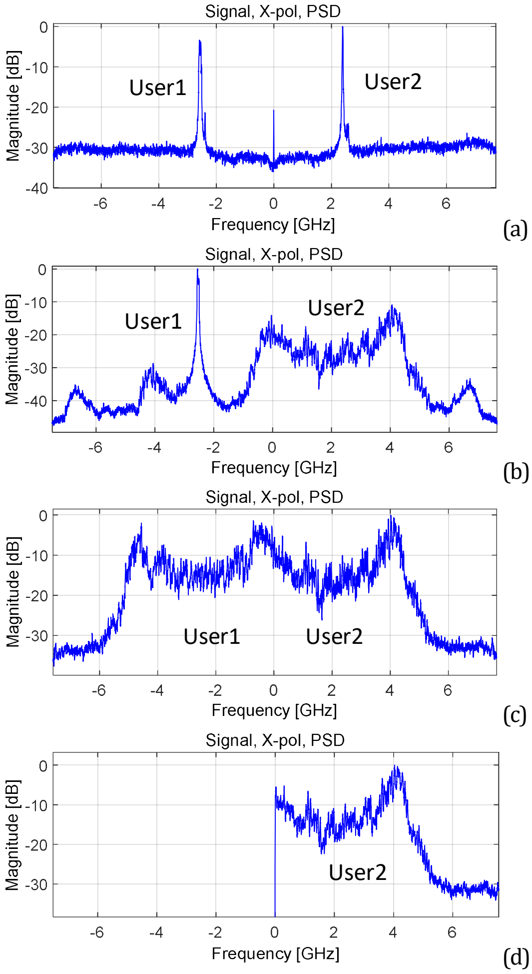

Fig. 11: Electrical spectrum of the complex I+jQ signal after photodetection at the 3x3 image-rejection RX, with IF = 2.5 GHz: (a) unmodulated users, (b) User 2 modulated with NRZ at 1.25 Gb/s, (c) both users modulated with NRZ at 1.25 Gb/s, and (d) User 2 after cancellation of User 1 by the image-rejection RX.

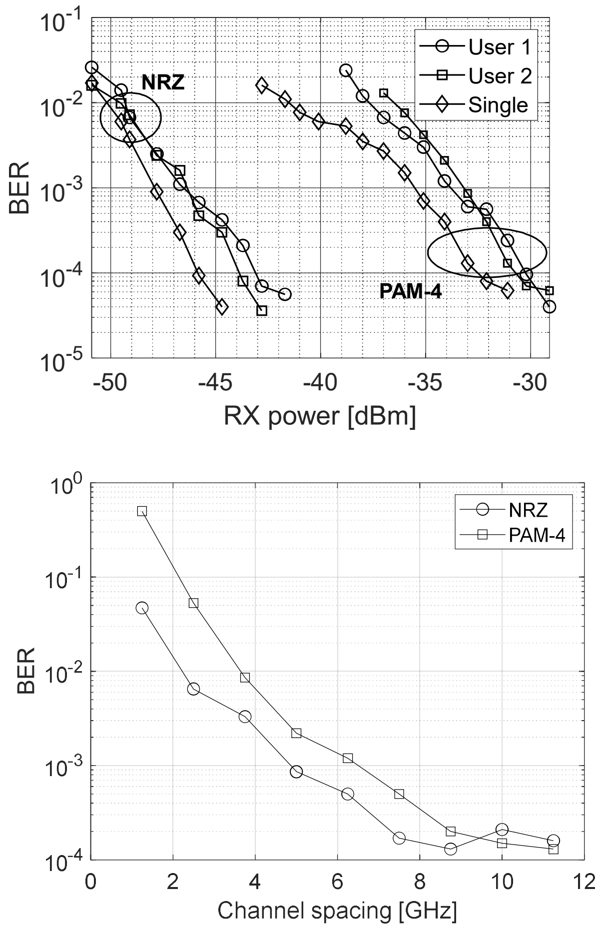

Fig. 12: For two users at 1.25 GBd with NRZ and PAM-4 in BB, detected simultaneously by the 3x3 heterodyne IR RX: (a) BER vs. RX power; (b) BER vs. channel spacing, the LO is placed in middle of the two users ($\Delta\lambda=2IF$).

Figure 12 (a). The bit rates are 1.25 and 2.5 Gb/s for NRZ and PAM-4, respectively. The IF = 2.5 GHz, and the users' separation $\Delta\lambda$ = 5 GHz. Notably, the two users are simultaneously detected with similar performances for each modulation format. The RX sensitivities at BER = 10^{-3} are -46 and -34 dBm for NRZ and PAM-4 respectively, which are correspondingly 2 and 1.5 dB worse than the single-user tests with NRZ in section 4.B.1 and PAM-4 in section 4.B.2, detected by the 3x3 homodyne RX single-polarization. These results very well match the results in [9] with NRZ using DMLs. The sensitivity penalty at BER = 10^{-3} for PAM-4 with respect to NRZ, with Δλ = 5 GHz, is about 12 dB in part by the Nyquist shaping and in part by the image-rejection at the RX that performs better as the IF increases, and is slightly worse for PAM-4. This behavior was experimentally evaluated in Figure 12 (b), which plots the BER as a function of the wavelength spacing Δλ between the two users. It is worth nothing that Δλ=2IF for the simultaneous detection of both users by the same heterodyne RX. The results show that for NRZ and PAM-4 users at 1.25 GBd, the minimum channel spacing for 1 dB penalty at BER = 10^{-4} is about 6.5 and 7.5 GHz respectively, to deal with the laser chirp spectrum spreading. All results are summarized in Table 5.

B. RF modulation

In the second scenario, the two users emit at the same wavelength and are multiplexed in electrical SCM through RF modulation of the lasers, as illustrated in Figure 13 (a). The users modulated NRZ and PAM-4 data at 625 MBd, on RF carriers at 1.25 and 3.75 GHz for User 1 and User 2 respectively. Yet, the RF frequencies were later varied to evaluate the minimum SCM channel separation Δf.

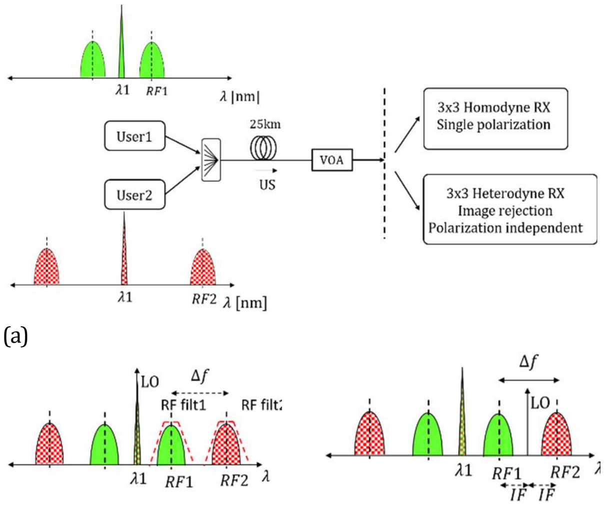

Fig. 13: (a) Continuous multiple access with two SCM users modulated in RF and detected simultaneously by (b) the 3x3 homodyne RX and (c) the 3x3 heterodyne image-rejection RX.

Table 6	
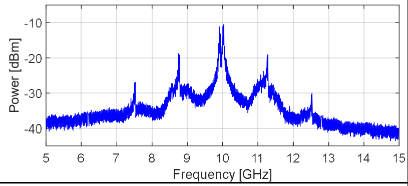	User1: ON. RF1 = 1.25 GHz User2: OFF.
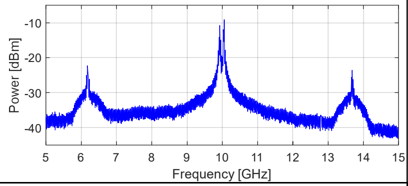	User1: OFF. User2: ON. RF2 = 3.75 GHz
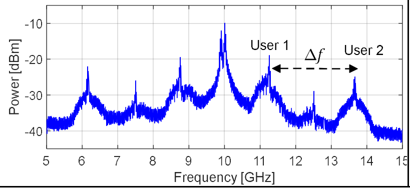	User1 and User 2 active. Users separation Δf = 2.5 GHz

	Table 5				
	IR Heterodyne Rx (Pol. Indep.) Sensitivity (dBm)				Δλ (GHz)
	Single	User 1	User 2	Penalty btw users	
NRZ	-48	-46	-46	0 dB	6.5
PAM-4	-35.5	-34	-33	1 dB	7.5
Penalty (dB)	12.5	12			>5RB (NRZ)

On the RX side, two coherent RX types were tested, for the sake of performance compassion. On the one hand, the two users were simultaneously detected by the 3x3 homodyne RX single-polarization used in Section 4. The LO was tuned at the same wavelength ($\lambda1$) than the two TXs for optical homodyne detection, and the RF User 1 and User 2 were demultiplexed by electrical band-pass filters, as shown in Figure 12 (b) On the other hand, the two users were also detected by the 3x3 heterodyne image-rejection RX, polarization-independent, by locating the LO in between of the two RF users as depicted in Figure 12 (c) and similar to the previous baseband modulation in Section 5.A. In this case, the RF users demultiplexing is carried out by the image-rejection part of the RX DSP.

Using the spectral configuration in Table 6, with R_B = 625 MBd, User 1 at RF1 = 1.25 GHz and User 2 at RF2 = 3.75 GHz, the BER curves were measured using the homodyne and the heterodyne image-rejection RX, as reported in Figure 14 (a) and 14 (b), and summarized in Table 7 and 8, respectively. In terms of the RX sensitivity at BER = 10^{-3}, and considering first the User 1 at RF = 1.25 GHz, the 3x3 homodyne RX performed better, with -44.5 and -35 dBm RX sensitivity for NRZ and PAM-4 respectively. The sensitivity penalty for the 3x3 heterodyne image-rejection RX for the same User 1 was 2.5 and 3 dB, achieving -42 and -32 dBm sensitivity for NRZ and PAM-4. Theoretically, the image-rejection RX compensates the 3 dB penalty in sensitivity of the heterodyne detection compared with homodyne, due to cancelation of half the total noise BW.

	Table 7				
	Homodyne (Single pol.)				
	Rx sensitivity (dBm)				Δf (GHz) (U2)
	Single	User 1	User 2	Penalty	
NRZ	-44.5	-44.5	-41.5	3 dB	1.75
PAM-4	-36	-35	-31	4 dB	1.75
Penalty (dB)	8.5	9.5	10.5		>2.8 RB
RF1 = 1.25 GHz, RF2 = 3.75 GHz, RB= 625 Mbd					

	Table 8			
	Heterodyne (Pol. diversity.)			
	Rx sensitivity (dBm)			Δf (GHz) (U2)
	User 1	User 2	Penalty (dB)	
NRZ	-42	-41	1 dB	2.3
PAM-4	-32	-30	2 dB	2.25
Penalty (dB)	10	11		> 3.7 RB (NRZ)
RF1 = 1.25 GHz, RF2 = 3.75 GHz, RB= 625 Mbd				

In the experiment, however, the lower sensitivity of the 3x3 image-rejection RX originates from the larger insertion loss of the optical front-end (two extra PBSs + one unused branch of the 3x3 coupler). The experimental electrical spectrum after heterodyne detection of the two users modulated in RF, and centered at 10 GHz, is reported in Table 6 for PAM-4 at 1.25 Gb/s. The RF frequencies are 1.25 and 3.75 GHz for User 1 and User 2 respectively. The sensitivity penalty between NRZ and PAM-4 at the same R_B was of 9.5 and 10 dB for the homodyne and the heterodyne RX respectively, considering User 1. For the User 2 at RF =

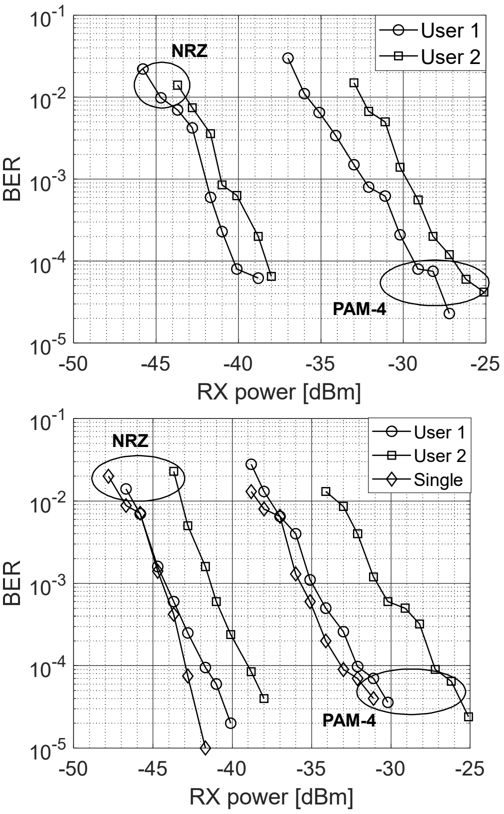

Fig. 14: BER vs. RX power for two SCM users at 625 MBd with NRZ and PAM-4, detected simultaneously by (a) the 3x3 homodyne RX and (b) the 3x3 heterodyne IR RX.

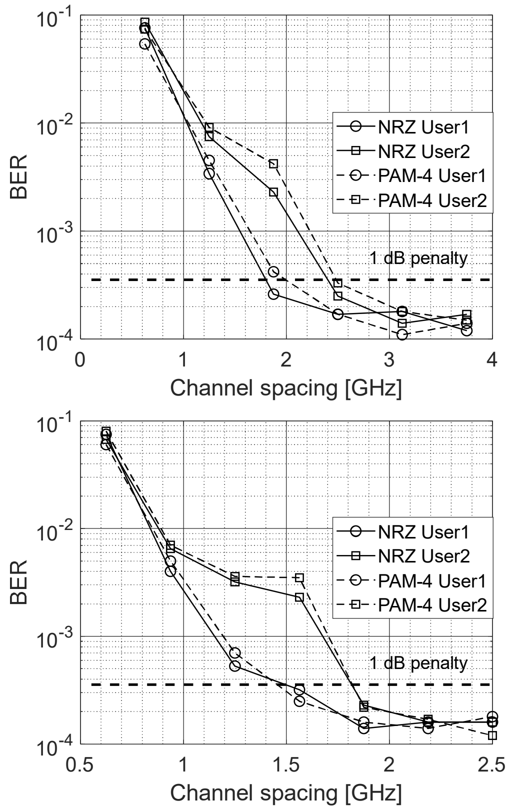

Fig. 15: BER vs. RF user separation for NRZ and PAM-4 at 625 MBd, detected by (a) 3x3 homodyne RX and (b) 3x3 heterodyne image-rejection RX. The RF of User 1 is fixed at 1.25 GHz and the RF of User 2 is swept to evaluate Δf.

3.75 GHz, detected by the homodyne RX, the penalties in sensitivity at BER = 10^{-3} with respect to User 1 were 3 and 4 dB for NRZ and PAM-4 respectively, because of the BW limitations and non-ideal frequency responses at higher frequencies. This matches well with the results in sections 4.C.1 and 4.C.2. Interestingly, the penalty between User 1 and User 2 with the same modulation format is lower in the heterodyne image-rejection RX, of about 1 and 2 dB for NRZ and PAM-4 respectively, mostly due to the lower required RX BW to detect the two users; thus, the total noise BW is lower and non-ideal frequency responses of the RX front-end have less impact.

The final tests aimed at comparing the required RF user separation Δf for the two coherent RX types. For the test, User 1 was fixed at RF = 1.25 GHz, then the RF frequency of User 2 was swept to evaluate the minimum Δf for 1 dB penalty in sensitivity at BER = 10^{-4}. Both users were detected simultaneously during the tests. The results are plotted in Figure 15 (a) and (b), respectively, and summarized in Tables 7 and 8.

From the test, it is interesting to note that the curves for RF User1 and User 2 are asymmetrical in all cases. The reason is that for Δf = 1.25 GHz the User 2 overlaps the second-order harmonic of the modulated User 1 (see Table 6), producing a penalty at the detection of User 2 but not in User 1. Taking as reference the largest RF separation required by the User 2, in homodyne detection with users demultiplexing by RF filtering the minimum Δf is 1.75 GHz for 1 dB penalty, whereas for heterodyne detection with image-rejection for users demultiplexing the minimum Δf is 2.3 GHz, which represents 30% larger RF users spacing due to the heterodyne detection. Moreover, by considering the novel 3x3 heterodyne image-rejection RX, polarization independent, and comparing the required separation between RF users in Figure 15 with respect to the baseband users in Figure 12, it can be seen that for base-band users at 1.25 GBd the users separation is >6 GHz, or $\Delta\lambda > 5R_B$. In contrast, for RF users at 625 MBd the RF separation is >2.3 GHz, or $\Delta f > 4R_B$, which is lower than in base-band modulation due to the narrower modulated spectral width mainly dictated by the laser chirp.

6. Discussion and conclusions

In this work, direct modulation tests have been carried out both in single user scenarios and with two simultaneous users in CMA configuration, baseband NRZ at 1.25 Gb/s and PAM-4 at 2.5 Gb/s were evaluated using coherent detection. The achieved sensitivities for BER = 10^{-3} were -49 and -42 dBm respectively, outperforming by 13 dB the highest sensitivity of actual standards for PON using TDM and direct detection, with NRZ at the same bit rate. The use of Nyquist pulse-shaping with roll-off = 1 showed a 1 dB penalty in sensitivity with respect to square pulse-shape. The penalty for PAM-4 with respect to NRZ at the same baud rate ranged from 7 to 12 dB depending on the pulse-shape filter, modulation index, and bit rate. The two modulation formats were also successfully demonstrated over electrical RF carriers up to 3.75 GHz, for data at 625 MBd. It is worth mentioning that the error-free detection of PAM-4 required a 4-tap FIR equalizer at the RX to compensate for the non-ideal frequency responses.

From these modulation tests, two different multiplexing techniques were evaluated for continuous high-speed optical access: UD-WDM users with baseband modulation, and SCM with user multiplexing by electrical RF subcarriers. In both cases, the detection was done by a novel coherent heterodyne RX, polarization independent, which rejects the image frequency band of the heterodyne detection, and compensates for the 3 dB loss in sensitivity with respect to the homodyne detection. The image-rejection characteristic of the heterodyne RX allowed to detect two different users simultaneously with the same RX and within the same electrical BW. The obtained results indicated that multiplexing the users in electrical RF required adjacent users separation of $\Delta f > 4R_B$, less than the separation required in wavelength multiplexing with baseband modulation, that needed $\Delta\lambda > 5R_B$ due to the laser chirp spectral spreading, which affects more in base-band than in RF modulation.

As final remarks, the baseband Tx with heterodyne IR Rx matched the same spectral efficiency than conventional homodyne, but detecting 2 users with the same LO and electrical bandwidth. When using the SCM, single wavelength PON, heterodyne IR achieved 52% less Rx bandwidth than homodyne Rx, as expected, with a penalty below 3 dB in sensitivity with respect the single polarization homodyne, being the heterodyne polarization independent. Finally, the homodyne Rx achieved 30% less channel spacing than the heterodyne IR.

That being said, all scenarios are useful as per different applications. The baseband Tx -heterodyne IR combination seems best when transceivers can afford a laser per transmitted channel, while SCM seems best in order to send multiple channels using the same optical source. If the OLT can afford a dedicated LO per ONU, heterodyne-IR has better compromises, mainly in terms of bandwidth, while the conventional homodyne is interesting for LO reuse of the same wavelength. The overview of the option compromises is summarized in Table 9.

	Table 9		
	1: BB-Het IR	2: SCM-Het IR	3: SCM-Hom
TX complexity	Lowest	Intermediate	Intermediate
Rx Complexity	Lowest	Lowest	High (if pol. independent)
Sensitivity	Highest	Intermediate	Lowest (if pol. independent)
User separation	Highest (chirp spreading)	Close to lowest	Lowest
Rx BW	Close to the highest	Lowest	Highest

References

1. L. Antão, R. Pinto, J. Reis and G. Gonçalves, "Requirements for Testing and Validating the Industrial Internet of Things," 2018 IEEE International Conference on Software Testing, Verification and Validation Workshops (ICSTW), 2018, pp. 110-115, doi: 10.1109/ICSTW.2018.00036.
2. N. Brahmi, O. N. C. Yilmaz, K. W. Helmersson, S. A. Ashraf and J. Torsner, "Deployment Strategies for Ultra-Reliable and Low-Latency Communication in Factory Automation," 2015 IEEE Globecom Workshops (GC Workshops), 2015, pp. 1-6,
3. Ernst & Young, "White paper: The backbone of digital economies: the revolution of global industries through optical communications" (2021)
4. D. Welch et al., "Point-to-Multipoint Optical Networks Using Coherent Digital Subcarriers," in Journal of Lightwave Technology, vol. 39, no. 16, pp. 5232-5247, 15 Aug.15, 2021, doi: 10.1109/JLT.2021.3097163.
5. J. Tabares and J. Prat, "Low-Complexity Phase-and-Polarization-Diversity Coherent Receiver with High Spectral Efficiency for UDWDM," in Proc. Opt. Fiber Commun. Conf. Exhib., 2021 (OFC), Paper Th5I.2.
6. ITU-T G.989.2 Recommendation: "40-Gigabit-capable Passive Optical Networks (NG-PON2): Physical media dependent (PMD) layer specification", Feb. 2019.
7. J. Tabares et al., "Simplified carrier recovery for intradyne optical PSK receivers in udWDM-PON," J. Lightw. Technol., vol. 36, no. 14, pp. 2941–2947, Jul. 2018.
8. J. C. Velásquez, J. Tabares, and J. Prat, "Differential 8-APSK monolithically integrated dualEML transmitter for flexible coherent PONs," Opt. Lett., vol. 44, no. 11, pp. 2760–2763, Jun. 2019.
9. M. Presi, R. Corsini, M. Artiglia, E. Ciaramella" Using directly modulated DFBs without power penalty in low-cost and high-power budget coherent access networks" in Electronics Letters, vol. 50, no 7, pp 536-538. DOI: 10.1049/el.2014.0096